

Gamma-Ray Constraints on Neutralino Dark Matter Clumps in the Galactic Halo

Roberto Aloisio

*INFN - Laboratori Nazionali del Gran Sasso
SS. 17bis, Assergi (AQ), ITALY*

and

*Center for Cosmological Physics
The University of Chicago, Chicago, IL 60637, USA*

roberto.aloisio@lngs.infn.it

Pasquale Blasi

*INAF - Osservatorio Astrofisico di Arcetri
Largo E. Fermi, 5 - 50125 Firenze, ITALY*

and

*Center for Cosmological Physics
The University of Chicago, Chicago, IL 60637, USA*

blasi@arcetri.astro.it

Angela V. Olinto

*Department of Astronomy & Astrophysics, & Enrico Fermi Institute,
The University of Chicago, Chicago, IL 60637, USA*

and

*Center for Cosmological Physics
The University of Chicago, Chicago, IL 60637, USA*

olinto@oddjob.uchicago.edu

ABSTRACT

According to high resolution cold dark matter (CDM) simulations, large virialized halos are formed through the constant merging of smaller halos formed at earlier times. In particular, the halo of our Galaxy may have hundreds of dark matter clumps. The annihilation of dark matter particles such as the neutralino in these clumps generates γ -ray fluxes that can potentially be detected by future experiments such as GLAST. We find that, depending on the parameters of the

clump density profile and on the distribution of clumps in the Galactic halo, the contribution to the diffuse γ -ray background from clumps can constrain the properties of neutralinos such as the mass and annihilation cross section. We model the density profile of clumps by three representative dark matter profiles: singular isothermal spheres (SIS), Moore profiles, and Navarro, Frenk and White (NFW) density profiles and calculate the spectrum and angular distribution in the sky of the γ -ray flux due to neutralino annihilation in the clumpy halo of the Galaxy. The calculations are carried out in the context of two different scenarios for the distribution of clumps in the Galaxy and their concentrations, which result in very different conclusions.

Subject headings: none supplied

1. Introduction

Most of the matter in the universe has yet to be observed in any frequency band, thus the name, dark matter (DM). The evidence for the predominance of dark over visible matter comes mainly from the gravitational effects of the dark matter component. However, gravitational studies have been unable to shed light on the nature of the dark matter. Big bang nucleosynthesis constrains most of the dark matter to be of non-baryonic origin. This has encouraged the study of plausible new particle candidates for the dark matter. The best motivated among these candidates is the lightest supersymmetric particle, named the neutralino, χ . Given the requirements of neutralino production in the early universe, it is possible to study the phenomenology of such dark matter candidates in detail (see, e.g., Jungman, Kamionkowski, and Griest 1996). In particular, the annihilation of neutralinos has often been considered a potential source of detectable secondaries: high energy particles and electromagnetic radiation. In this sense, dark matter can be visible through the radiation caused by the annihilation secondaries (Berezinsky, Gurevich and Zybin 1992; Berezinsky, Bottino and Mignola 1994; Gondolo and Silk 1999; Bergström et al. 1999; Gondolo 2000; Calcáneo-Roldán and Moore 2000; Bertone, Sigl and Silk 2001; Bergström, Edsjö and Ullio 2001; Blasi, Olinto and Tyler 2002; Tyler 2002; Ullio et al. 2002; Tasitsiomi and Olinto 2002; Cesarini et al. 2003).

Recent advances in cold dark matter (CDM) simulations have shown that the large scale structure of the universe can be explained in terms of a hierarchical scenario in which large halos of dark matter are generated by the continuous merging of smaller halos (Ghigna et al. 1998; Moore et al. 1999; Klypin et al. 1999). In this picture, a dark matter halo is the superposition of a smooth component on a scale comparable with the virial radius of the

forming structure and a clumped structure made of thousands of smaller mass halos. As we discuss below, this scenario can have important consequences for the detection of signals from neutralino-antineutralino ($\chi\bar{\chi}$) annihilation.

CDM simulations also show that most halos are well described by a density distribution with cusps at the center of each halo. The exact shape of the central cusp is still a matter of debate. Most recent simulations favor profiles with density cusps varying from the Moore et al. profile (Moore et al. 1999) where $\rho_{DM}(r \rightarrow 0) \sim r^{-1.5}$ to a Navarro, Frenk, and White (NFW) profile (Navarro, Frenk and White 1996) where $\rho_{DM}(r \rightarrow 0) \sim r^{-1}$ (see also Power et al. 2002). The more concentrated the central cusp, the easier to detect annihilation products since the annihilation rate is proportional to the square of the dark matter density. The existence of cuspy halos is still unclear since observations of galaxy rotation curves provide no evidence of central cusps (see, e.g., Salucci 2001). However, the survival of cusps in galactic centers is highly dependent on the galaxy’s merger history in particular on the history of formation of galactic center black holes (Merrit and Milosavljevic 2002). The central regions of small mass dark matter halos (i.e., DM clumps) are less affected by the dynamics of baryonic matter and less likely to have black hole mergers at their centers. Thus, a cuspy profile may well describe the density of DM clumps.

Another important piece of information is embedded in the spatial distribution and survival history of clumps on their way to the central part of the host galactic halo. Tidal interactions significantly affect clump distribution and structure and these effects are only beginning to be resolved in CDM simulations for relatively large mass clumps (Stoehr et al. 2002). Given the lack of a clear understanding of present distribution of DM clumps in the Galaxy halo, we consider two different scenarios that bracket the present uncertainties. For simplicity we call these two approaches type I and type II. We show that the present uncertainties lead to large variations in the resulting gamma-ray signal.

In the type I scenario, the clump position in the host Galaxy determines its external radius. In the case of NFW and Moore profiles, the location of the core is then determined by assuming a fixed fraction of this external radius. In the type II scenario, the concentration parameter, defined as the ratio of the core radius to virial radius of a clump, is modeled as in Wechsler et al. (2001) for clumps for a given mass. We show that in this scenario the clumps are gradually destroyed on their way to the center of the Galaxy, such that the inner part of the Galactic halo is depleted of clumps. This second scenario seems compatible with numerical simulations (Power et al. 2002, Stoehr et al. 2002). The uncertainties on clump distribution and concentration bracketed by these two scenarios strongly affect the resulting γ -ray emission from the annihilation of neutralinos: while in the type I scenario, the highly concentrated clumps produce strong γ -ray emission, in the type II scenario the

low concentration clumps imply γ -ray fluxes several orders of magnitude smaller.

The paper is structured as follows: in section 2 we introduce the clump density profiles; in section 3 we discuss the distribution of clumps in the Galaxy and the calculations of the gamma ray flux; in section 4 we present our results, consisting of the spectra and anisotropies of the γ -ray emission in the type I and II scenarios, for different shapes of the clumps density profiles. We conclude in section 5.

2. Dark Matter Clumps in the Halo

The contribution to the diffuse γ -ray background from $\chi\bar{\chi}$ annihilation in the clumpy halo depends on the distribution of clumps in the halo and on the density profile of clumps. Our purpose here is to investigate the wide variety of possibilities currently allowed by the results of simulations and suggested by some theoretical arguments, concerning the density profiles of dark matter clumps. We consider three cases: singular isothermal spheres (SIS), Moore et al. profiles, and NFW profiles.

The Moore et al. and the NFW profiles are both the result of fits to different high resolution simulations (Moore et al. 1999, Power et al. 2002). Although there is ongoing debate over which profile is most accurate, it is presently believed that a realistic descriptions of the dark matter distribution in halos will follow a profile in the range defined by the Moore et al. and the NFW fits (see, e.g., Tasitsiomi 2002).

The dark matter density profiles can be written as follows:

$$\rho_{\chi,\text{SIS}}(r) = \rho_0 \left(\frac{r}{r_0} \right)^{-2}. \quad (1)$$

$$\rho_{\chi,\text{Moore}}(r) = \frac{\rho_0}{\left(\frac{r}{r_f} \right)^{3/2} \left[1 + \left(\frac{r}{r_f} \right)^{3/2} \right]} \quad (2)$$

$$\rho_{\chi,\text{NFW}}(r) = \frac{\rho_0}{\left(\frac{r}{r_f} \right) \left(1 + \frac{r}{r_f} \right)^2}. \quad (3)$$

The SIS and Moore et al. clump density profiles are in the form given in eqs. (1) and (2) down to a minimum radius, r_{\min} . Inside r_{\min} , neutralino annihilations are faster than the cusp formation rate, so that $\rho(r \leq r_{\min}) = \rho(r_{\min})$ remains constant. To estimate r_{\min} , following Berezhinsky, Gurevich and Zybin 1992, we set the annihilation timescale equal to the free-fall timescale, so that

$$r_{\min,\text{SIS}} = r_0 \left(\frac{\langle \sigma v \rangle \rho_0}{\sqrt{GM_c} m_\chi} r_0^{3/2} \right)^{1/2}, \quad (4)$$

$$r_{\text{min,Moore}} = r_0 \left(\frac{\langle \sigma v \rangle_{\chi\bar{\chi}}^2 \rho_0^2}{GM_c m_\chi^2} r_f^3 \right)^{1/3}, \quad (5)$$

where $\langle \sigma v \rangle_{\chi\bar{\chi}}$ is the $\chi\bar{\chi}$ annihilation cross-section, G is Newton's constant, and M_c and m_χ are respectively the clump mass and the neutralino mass.

We modeled the smooth galactic halo density with a NFW density profile (eq. (3)), with $r_f = 27$ kpc and ρ_0 determined by the condition that the dark matter density at the Sun's position be $\rho_{DM}(d_\odot) = 6.5 \times 10^{-25} \text{g/cm}^3$.

The fundamental parameters of the clump density profile are the density normalization ρ_0 , the clump radius r_0 and, in the case of Moore et al. and NFW profiles, the clump fiducial radius r_f . In order to fix these fundamental parameters we have considered two different scenarios (type I and II).

In the type I scenario, the radius of a clump with fixed mass is determined by its position in the Galactic halo. More specifically, the radius of the clump is located at the radius where the clump density equals the density of the Galactic (smooth) dark matter halo at the clump position (namely ρ_0). The physical motivation for such a choice is to account for the tidal stripping of the external layers of the clump while the clump is moving in the potential of the host halo. For the NFW and Moore profiles, the fiducial radius r_f has been taken as a fixed fraction of r_0 : $r_f = 0.1r_0$.

In the type II scenario the external radius of the clumps is taken to be their virial radius, defined in the usual way:

$$r_0 = r_{\text{vir}} = \left(\frac{3M_c}{4\pi\rho_{200}} \right)^{1/3}, \quad (6)$$

where ρ_{200} is 200 times the critical density of the Universe $\rho_c = 1.88 \times 10^{-29} h^2 \text{g/cm}^3$ (we assume $h = 0.7$). In this scenario, following Ullio et al. 2002, we have introduced the concentration parameter defined as

$$\xi = \frac{r_0}{r_{-2}} \quad (7)$$

where r_{-2} is the radius at which the effective logarithmic slope of the profile is -2 , set by the equation

$$\frac{1}{\rho_0} \frac{d}{dr} r^2 \rho(r) = 0 .$$

The mass dependence of the concentration parameter used in our calculations is taken from Wechsler et al. 2001, and is plotted in fig. 1 for the present time (zero redshift). The general trend is for smaller clumps to have larger concentration parameter, reflecting the fact that they were formed at earlier epochs, when the universe was denser.

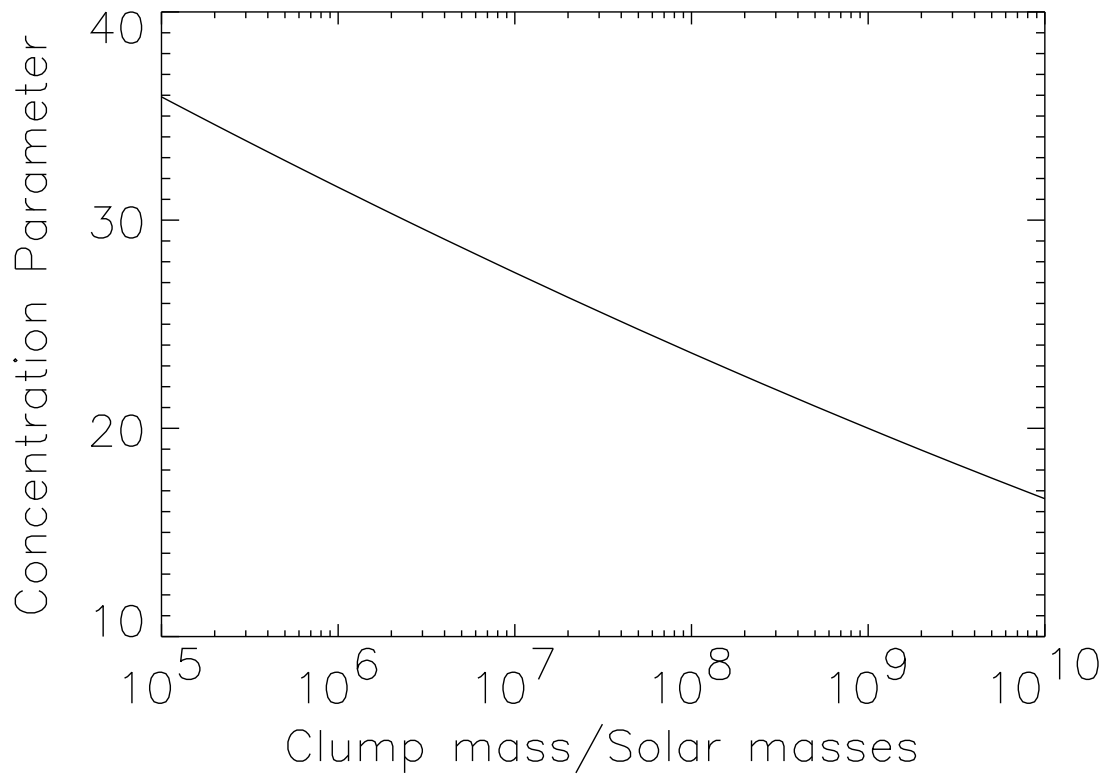


Fig. 1.— Concentration parameter for dark matter clumps, as a function of the clump mass.

The normalization constant in the clump density profile ρ_0 is fixed recalling that the clump mass M_c is

$$M_c = \int_0^{r_0} 4\pi r^2 \rho_\chi(r) dr .$$

In the case of the NFW density profile, $r_f = r_{-2}$, while in the case of the Moore et al. density profile, $r_f = r_{-2}/0.63$ (Ullio et al. 2002). In terms of concentration parameters

$$\xi_{NFW} = 0.63 \xi_{Moore} . \tag{8}$$

Using the concentration parameter plotted in fig. 1 for NFW clumps, we can estimate a stripping distance, which we define as the distance from the galactic center where the density of a clump at the fiducial radius r_f equals the density in the smooth halo. At the stripping distance, layers of the clump outside the fiducial radius are stripped off by the Galactic halo tidal forces. The stripping distance defined in this way is plotted in fig. 2.

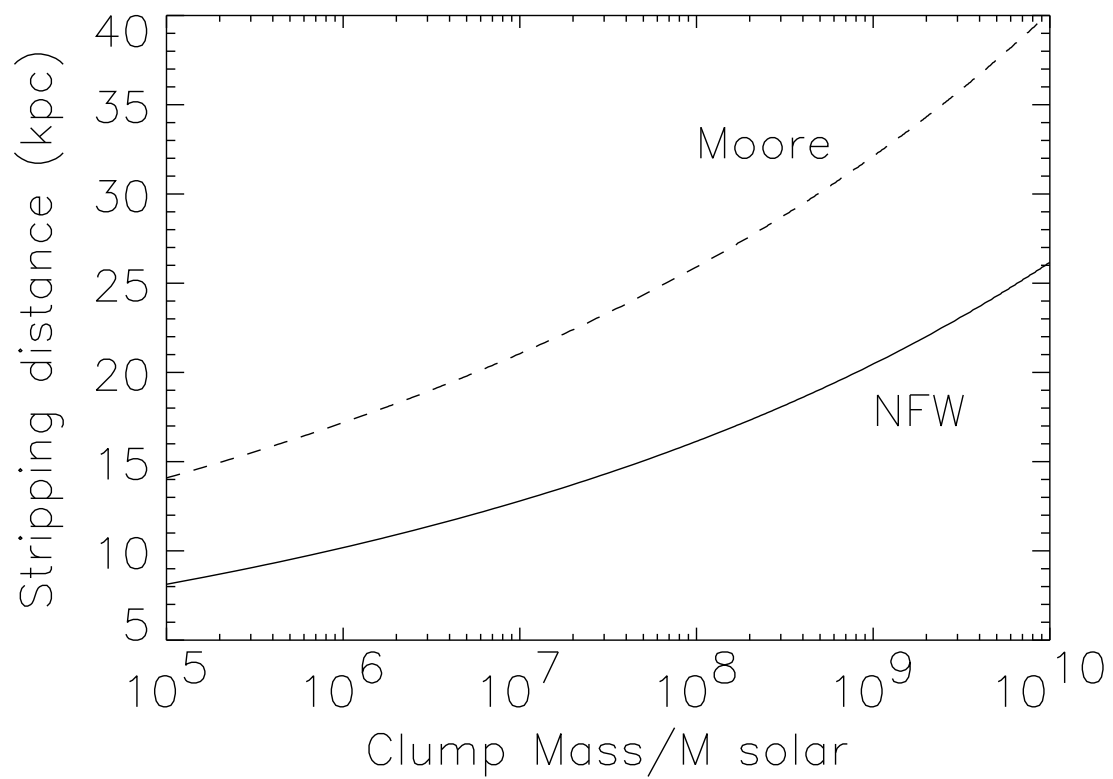


Fig. 2.— Stripping radius of clumps as a function of the clump mass, for NFW and Moore density profiles.

From this estimate it is easy to see that most clumps in the inner parts of the host halo are stripped of most of their mass, so the number of clumps in the inner regions is very low. In fact, most clumps that are able to reach the central part of the Galaxy merge with the smooth dark matter profile. Only relatively lower mass older clumps can reach closer to the inner regions without significant disruption since they are in general more concentrated and have denser cores. Numerical simulations show the disappearance of large clumps in the centers of galaxy size halos, but they cannot resolve the smaller mass clumps that may eventually make their way into the core of the galaxy. In order to bracket the plausible range in clump distributions, we make the very conservative assumption in scenario II that the inner 10 kpc of the Galaxy halo have no clumps at all.

3. Gamma-ray emission

In order to determine the gamma ray emission from the DM clumps, we model the distribution of clumps in the Galaxy with a fit to numerical simulations as in Blasi and Sheth (2000). The probability distribution function of clumps with a given mass and at a given position d (measured from the Galactic center) is given by:

$$N_c(d, M_c) = N_{c,0} \left(\frac{M_c}{M_H} \right)^{-\alpha} \left(1 + \left(\frac{d}{d_{sc}} \right)^2 \right)^{-3/2}, \quad (9)$$

where $N_{c,0}$ is a normalization constant and d_{sc} is the scale radius of the clump distribution (assumed to be 10 kpc as in Blasi and Sheth 2000). Simulations find $\alpha \simeq 1.9$ and a halo like that of our Galaxy, with $M_H \simeq 2 \times 10^{12} M_\odot$, contains about 500 clumps with mass larger than $10^8 M_\odot$ (Ghigna et al. 1998).

The gamma ray flux per unit solid angle and per unit energy along a fixed line of sight in the (θ, ϕ) direction can be computed as

$$\Phi_\gamma(E_\gamma, \theta, \phi) = \frac{1}{4\pi} \int_0^{s_{max}} ds \int_{M_{min}}^{\zeta M_H} N_c(d(s), M) \mathcal{N}_\gamma dM \quad (10)$$

where $d(s) = \sqrt{s^2 - 2sd_\odot \cos\theta + d_\odot^2}$ is the distance of a generic point on the line of sight from the Galactic center (with θ as the angle between the direction s and the axis Sun-Galactic center), M is the clump mass, ζM_H is the maximum allowed mass for DM clumps in the Halo. We use $\zeta = 0.01$, since the Milky Way halo does not show recent mergers of satellites with masses larger than $\sim 2 \times 10^{10} M_\odot$ (the Large Magellanic Cloud has about $9 \times 10^9 M_\odot$). \mathcal{N}_γ is the total number of photons emitted per unit time and energy by a DM clump of mass M . This quantity, depending on the scenario chosen for the clump density

profile, may depend or not on the distance $d(s)$ of the considered point from the Galactic center. In the first scenario, where the normalization of the clump density is related to the smooth Halo density, $\mathcal{N}_\gamma = \mathcal{N}_\gamma(M, d, E_\gamma)$, while in the second scenario $\mathcal{N}_\gamma = \mathcal{N}_\gamma(M, E_\gamma)$. Note that eq. (10) is an average over all possible realizations of a halo with its clumpy structure. Fluctuations around this value may be present due to the accidental proximity of a few clumps in the specific realization that we happen to experience in our Galaxy.

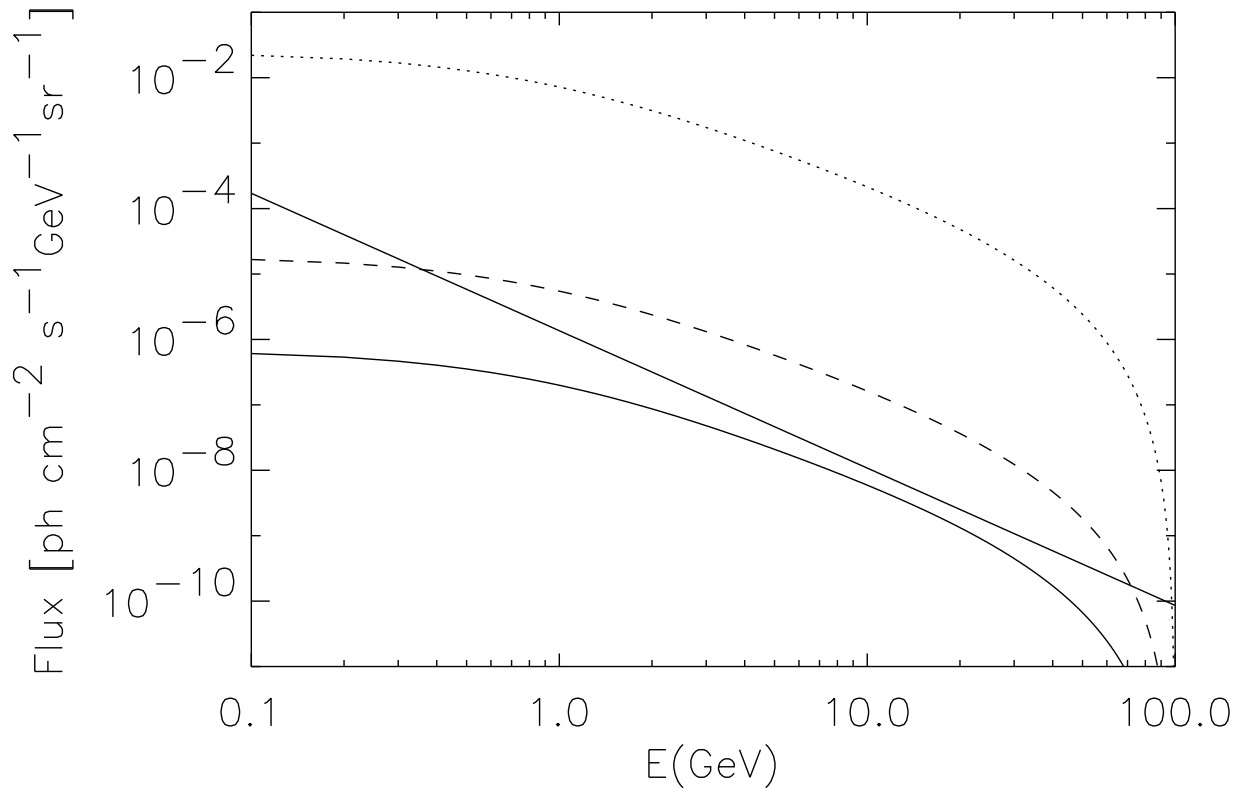


Fig. 3.— Type I scenario. Flux of gamma-rays in units of $(\text{GeV cm}^2 \text{s sr})^{-1}$ arriving on Earth averaged in all directions for $m_\chi = 100 \text{ GeV}$, $\langle\sigma v\rangle = 3 \times 10^{-27} \text{ cm}^3/\text{s}$ and $M_{c,min} = 10^5 M_\odot$. SIS density profile (dotted line), Moore et al. density profile (dashed line) and NFW density profile (continuous line). Also shown is the EGRET data on extragalactic diffuse gamma-ray background (Sreekumar 1998)

In principle, the neutralino annihilation production of gamma-rays has a complex spectrum with contributions from a number of channels (for a recent example, see Cesarini et al. 2003). Given that the uncertainties in the clump concentration induce very large variations in the total gamma-ray flux, we chose to calculate the gamma-ray spectrum by considering the dominant gamma-ray emission due to π^0 production from quark-antiquark pairs and neglected leptonic and bosonic channels. With this simplifying assumption we derive gamma-ray spectra that are in good agreement with Ullio et al. (2002) and Cesarini et al. (2003) for m_χ less than the W-boson mass and for m_χ above the top quark mass. The discrepancy between the simplified spectra we derive below and the fit by Berstrom et al. (2001) vary slightly with neutralino parameters, but stay within a factor of a few for neutralino masses from 10 GeV up to a few TeV.

The number of photons produced by quark-antiquark pairs with energy E_γ in a single $\chi\bar{\chi}$ annihilation can be written as follows:

$$\frac{dN_\gamma}{dE_\gamma} = \int_{E_{\pi,\min}}^{E_{\pi,\max}} dE_\pi P(E_\pi, E_\gamma) \frac{dN_\pi}{dE_\pi} \quad (11)$$

where $P(E_\pi, E_\gamma) = 2(E_\pi^2 - m_\pi^2)^{-1/2}$ is the probability per unit energy to produce a γ -ray with energy E_γ out of a pion with energy E_π . For the pion fragmentation function we assume the functional form introduced in Hill (1983):

$$\frac{dN_\pi}{dE_\pi} = \frac{1}{m_\chi} \frac{15}{16} x^{-3/2} (1-x)^2 \quad (12)$$

with $x = E_\pi/m_\chi$, $E_{\pi,\max} = m_\chi$ and $E_{\pi,\min} = E_\gamma + m_\pi^2/4E_\gamma$. Finally,

$$\frac{dN_\gamma}{dE_\gamma} = \frac{5}{4m_\chi} \int_{x_m}^1 dx \frac{(1-x)^2}{x^{3/2}(x^2 - \eta^2)^{1/2}}, \quad (13)$$

where $\eta = m_\pi/m_\chi$, and $x_m = E_\gamma/m_\chi + m_\chi\eta^2/4E_\gamma$.

The neutralino annihilation rate per unit volume is,

$$\Gamma_{\chi\bar{\chi}}(r, M, E_\gamma) = \rho_\chi^2(r) \langle \sigma v \rangle / m_\chi^2,$$

therefore the γ -ray emissivity $j_\gamma(r, M, E_\gamma)$ associated with the single clump of mass M is obtained by multiplying eq. (13) by $\Gamma_{\chi\bar{\chi}}$. The number of gamma rays produced per unit time and per unit energy in a single DM clump of mass M is then

$$\mathcal{N}_\gamma(M, E_\gamma) = \int_0^{r_0} dr 4\pi r^2 j_\gamma(r, M, E_\gamma). \quad (14)$$

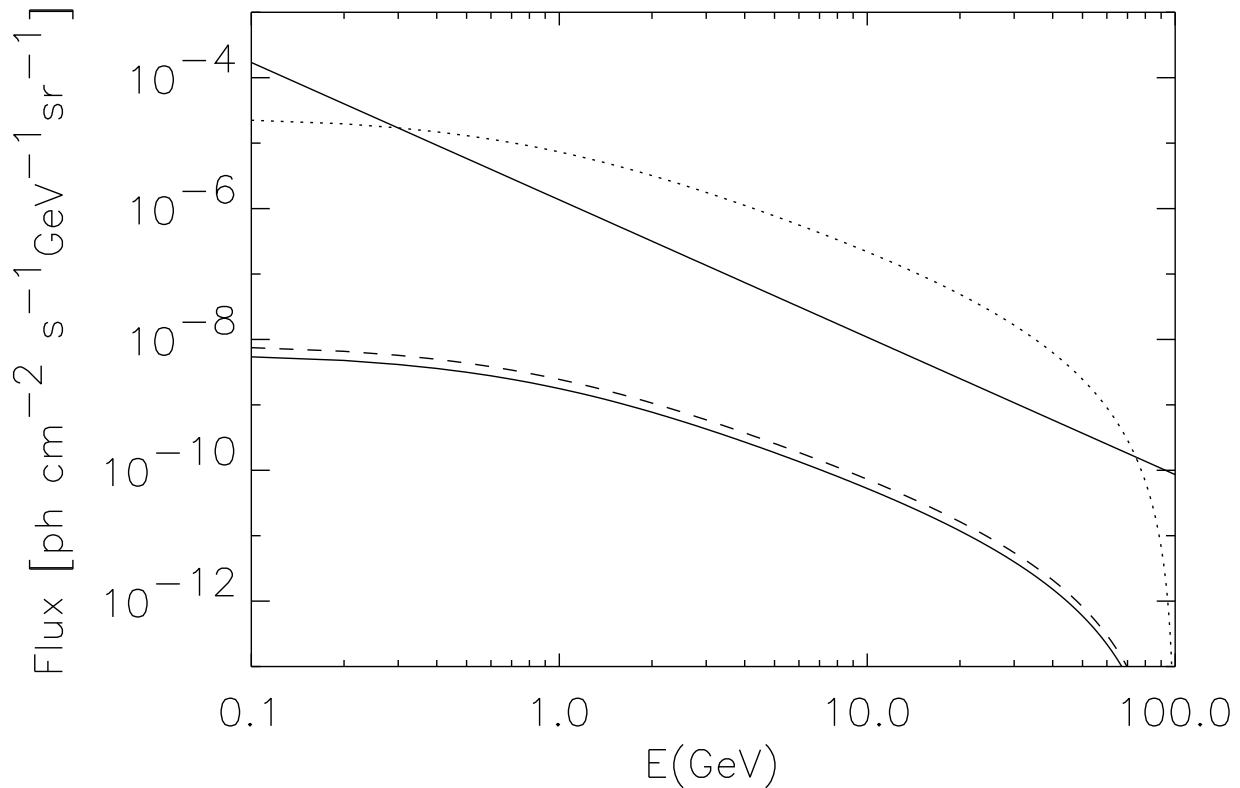


Fig. 4.— Type II scenario. Flux of gamma-rays in units of $(\text{GeV cm}^2 \text{ s sr})^{-1}$ arriving on Earth averaged in all directions for $m_\chi = 100 \text{ GeV}$, $\langle\sigma v\rangle = 3 \times 10^{-27} \text{ cm}^3/\text{s}$ and $M_{c,min} = 10^5 M_\odot$. SIS density profile (dotted line), Moore et al. density profile (dashed line) and NFW density profile (continuous line). The solid line is the EGRET bound on extragalactic diffuse gamma-ray background (Sreekumar 1998).

4. Results

In this section we present the γ -ray emission resulting from the dark matter annihilation in the halo of our Galaxy, including both the smooth and clumped components introduced above. We detail the description of these results for the two scenarios (type I and II) of spatial distribution and concentration of the clumped component. The emission in type II scenarios is much weaker than that obtained in type I scenarios, because type I clumps have much stronger concentration. In type II scenarios, the gamma ray signal from clumps overcomes the gamma ray flux from the smooth dark matter distribution only in the direction of the galactic anticenter and only for SIS and Moore profiles for the dark matter distribution inside the clumps. On the other hand, in type I scenarios the contribution of the clumped component to the diffuse gamma ray flux from the galactic halo is several orders of magnitude above the smooth halo component, for any of the three density profiles considered above. This impressive difference in the predictions is symptomatic of a large uncertainty in the formation and survival of dark matter substructures.

In figs. 3 and 4 we plot the flux of gamma-rays in type I and II scenarios in units of $(\text{GeV cm}^2 \text{ s sr})^{-1}$ arriving on Earth averaged in all directions for $m_\chi = 100 \text{ GeV}$ and with $\langle\sigma v\rangle = 3 \times 10^{-27} \text{ cm}^3/\text{s}$. The curves refer to the gamma ray flux due to the full dark matter halo including the smooth and the clumped components. In both figures the dotted, dashed and solid lines correspond to SIS, Moore and NFW clump density profiles respectively. The fluxes are obtained for a minimum clump mass of $M_{c,min} = 10^5 M_\odot$. The dependence of these fluxes on the value of $M_{c,min}$ is very weak. The diffuse flux is the convolution of the mass function of the clumps (slightly flatter than $\sim M^{-2}$) and the gamma flux from a single clump. For the three density profiles we study, the flux from a single clump scales as $\sim M$, thus the diffuse flux scales logarithmically with $M_{c,min}$.

For the type II scenario, the gamma-ray flux contributed by the clumped component is comparable to the contribution of the smooth dark matter profile, while for the type I scenario, the clumpy component is overwhelmingly larger than that due to the smooth component. Also shown is the EGRET bound on the extragalactic diffuse gamma-ray background (Sreekumar 1998), which is known from 30 MeV to $\sim 30 \text{ GeV}$ to fit:

$$\frac{dN_{eg}}{d\Omega dE} = 1.36 \times 10^{-6} \left(\frac{E}{\text{GeV}} \right)^{-2.10} \text{ GeV}^{-1} \text{ cm}^{-2} \text{ s}^{-1} \text{ sr}^{-1} . \quad (15)$$

Depending on the density profile the fluxes have different scalings with the neutralino parameters m_χ and $\langle\sigma v\rangle$:

$$\Phi_{SIS} \propto \langle\sigma v\rangle^{1/2} m_\chi^{-5/2} \quad \Phi_{NFW, Moore} \propto \langle\sigma v\rangle m_\chi^{-3} . \quad (16)$$

These scalings are the same for the type I and II scenarios.

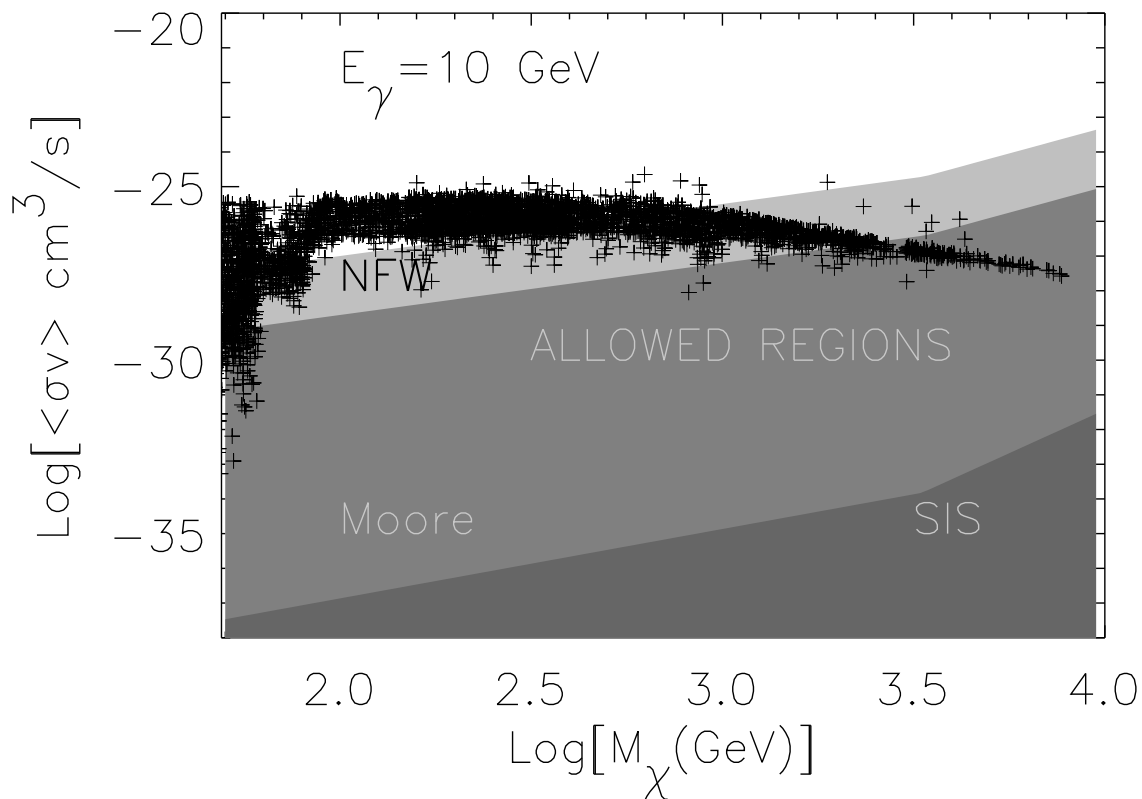


Fig. 5.— Neutralino cross section times velocity (thermally averaged) versus neutralino mass. Crosses are neutralino models from Tasitsiomi and Olinto (2002). Shaded regions are allowed regions of neutralino parameters for type I scenarios for clumps with the labeled dark matter profiles (NFW, Moore, SIS). Models with parameters above the shaded regions are ruled out by the EGRET diffuse flux in type I scenarios.

It is clear from figs. 3 and 4 that the comparison between our predictions and the observed diffuse background is meaningful only for the type I scenario, with highly concentrated clumps. In the second scenario, the fluxes are too low, with the exception of the case in which the density profile is the extreme SIS case. For the other profiles, the region of parameters that can be constrained is already ruled out from accelerator experiments $m_\chi \geq 50$ GeV (Hagiwara et al. 2002) and from theoretical arguments $\langle\sigma v\rangle \leq 10^{-26}\text{cm}^3/\text{s}$ (Baltz et al. 2002).

The situation is different for type I scenarios. As anticipated, all the density profiles imply gamma-ray fluxes comparable to or largely in excess of the EGRET observations of the diffuse gamma ray background. These observations may therefore be used to extract constraints on the neutralino parameter space. In fig. 5, we show the thermally averaged cross section times velocity of neutralinos as a function of neutralino mass. To give a sense of where neutralino parameters tend to lie in this graph we plot in crosses a set of $\langle\sigma v\rangle$ versus m_χ generated in DarkSUSY (P.Gondolo et al 2002) by Tasitsiomi and Olinto (2002). These models span a range of parameters in minimal supersymmetric extensions of the Standard Model (MSSM) and a range of cosmological dark matter densities consistent with observations. Note that the neutralino parameter space can generate an even smaller range of $\langle\sigma v\rangle$ versus m_χ for further constrained versions of MSSM, such as the constrained MSSM (CMSSM) where the neutralino masses is less than 500 GeV (Ellis et al. 2003) for a large range of MSSM parameters.

The shaded regions in fig. 5 show the allowed regions of parameters for different clump profiles in the type I scenario for clump concentration. Using the scalings given in eq. (16) and EGRET data at 10 GeV, we find that SIS clumps in our halo are ruled out in the region $\langle\sigma v\rangle \gtrsim 2 \times 10^{-35}(m_\chi/100\text{ GeV})^2\text{cm}^3/\text{s}$ for $50\text{ GeV} \leq m_\chi \leq 3\text{TeV}$, and $\langle\sigma v\rangle \gtrsim 6 \times 10^{-40}(m_\chi/100\text{ GeV})^5\text{cm}^3/\text{s}$ for $m_\chi \gtrsim 3\text{ TeV}$.

Moore et al. clumps are also strongly constrained: the 10 GeV EGRET data require that $\langle\sigma v\rangle \lesssim 2.5 \times 10^{-28}(m_\chi/100\text{ GeV})^{3/2}\text{cm}^3/\text{s}$ for $50\text{ GeV} \leq m_\chi \leq 3\text{ TeV}$, and $\langle\sigma v\rangle \lesssim 10^{-30}(m_\chi/100\text{ GeV})^3\text{cm}^3/\text{s}$ for $m_\chi \gtrsim 3\text{ TeV}$. If we extend eq. (15) from 30 GeV to 100 GeV assuming the same functional form, the bounds get tighter: for m_χ between 50 GeV and 30 TeV, the flux from clumps is below the γ -ray background if $\langle\sigma v\rangle \lesssim 6 \times 10^{-29}(m_\chi/100\text{GeV})^{3/2}\text{cm}^3/\text{s}$, while for $m_\chi \gtrsim 30\text{ TeV}$, the region $\langle\sigma v\rangle \lesssim 10^{-32}(m_\chi/100\text{GeV})^3\text{cm}^3/\text{s}$ is allowed.

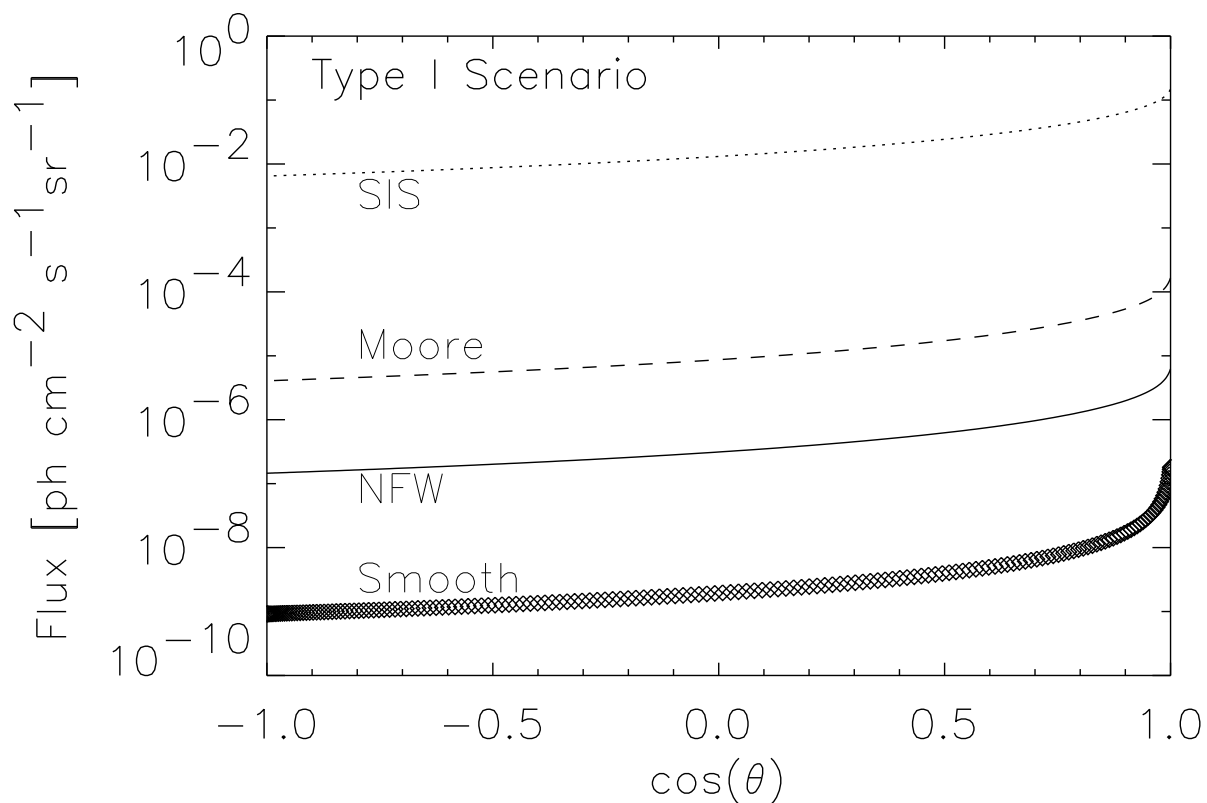


Fig. 6.— Dependence of the energy integrated gamma ray flux on the angle θ for the type I scenario. The solid, dashed and dotted lines refer to clumps with NFW, Moore and SIS density profiles respectively. The thick line is the contribution of the smooth component. A neutralino mass of 100 GeV and annihilation cross section of $3 \times 10^{-27} \text{ cm}^3/\text{s}$ have been used.

NFW clumps in the type I scenario are only weakly constrained. The bounds that can be placed by EGRET at 10 GeV are as follows: if m_χ is between 50 GeV and 3 TeV, the allowed region is defined by $\langle\sigma v\rangle \lesssim 10^{-26}(m_\chi/100\text{GeV})^{3/2} \text{ cm}^3/\text{s}$. For $m_\chi \gtrsim 3 \text{ TeV}$, the allowed region is instead $\langle\sigma v\rangle \lesssim 6 \times 10^{-29}(m_\chi/100\text{GeV})^3 \text{ cm}^3/\text{s}$. If we extrapolate eq. (15) from 30 GeV to 100 GeV, the bounds become: for m_χ between 50 GeV and 30 TeV, one must have $\langle\sigma v\rangle \lesssim 3 \times 10^{-27}(m_\chi/100\text{GeV})^{3/2} \text{ cm}^3/\text{s}$ while for $m_\chi \gtrsim 30 \text{ TeV}$, the allowed region becomes $\langle\sigma v\rangle \lesssim 5 \times 10^{-31}(m_\chi/100\text{GeV})^3 \text{ cm}^3/\text{s}$. All these bounds are shown in fig. 5.

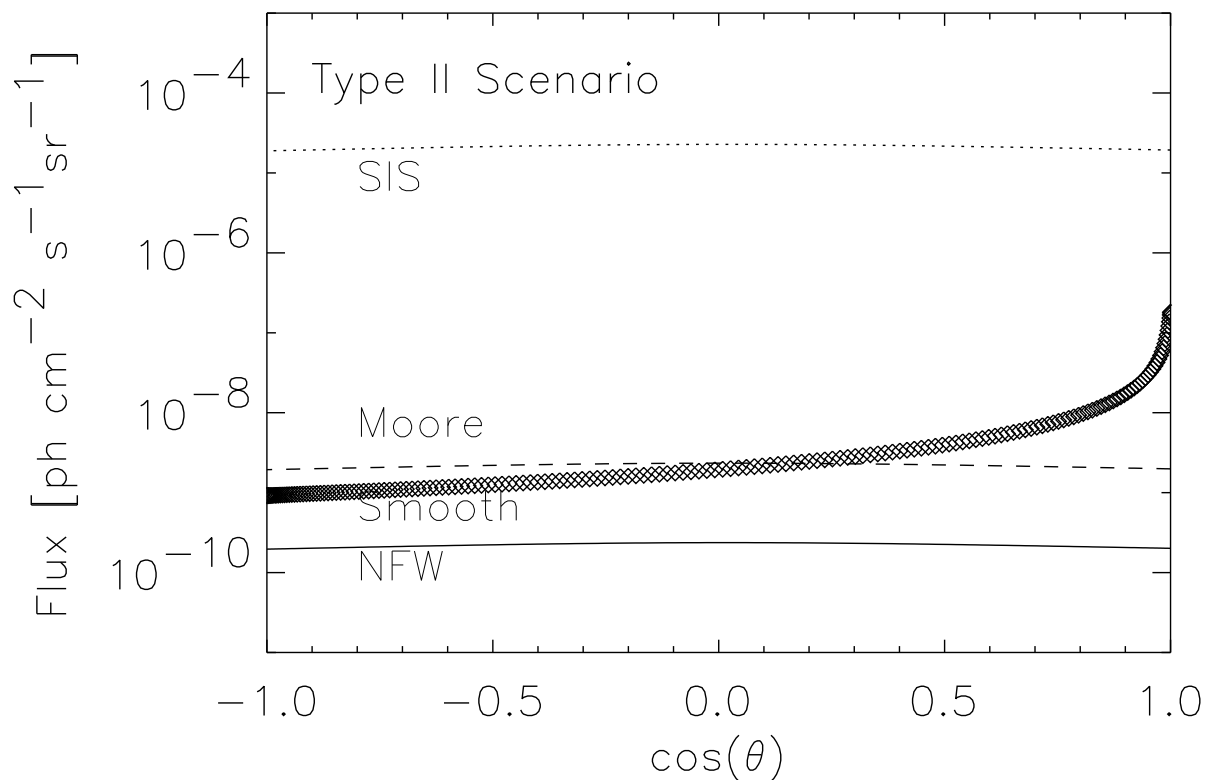


Fig. 7.— Dependence of the energy integrated gamma ray flux on the angle θ for the type II scenario. The solid, dashed and dotted lines refer to clumps with NFW, Moore and SIS density profiles respectively. The thick line is the contribution of the smooth component. A neutralino mass of 100 GeV and annihilation cross section of $3 \times 10^{-27} \text{ cm}^3/\text{s}$ have been used.

An important signature of the diffuse gamma ray emission from dark matter annihilation in the halo of our Galaxy is the anisotropy due to the off-center position of the solar system compared to the center of the dark matter distribution. The anisotropy for the type I and type II scenarios is shown in figs. 6 and 7 respectively, where we have plotted the energy integrated flux above 100 MeV versus $\cos(\theta)$ (equal to 1 in the direction of the galactic center). In these plots an isotropic flux would appear as a flat line. The energy integrated flux on the y-axis is defined as

$$I(\theta) = \frac{1}{2\pi} \int_{E_{\gamma, \min}}^{m_\chi} dE_\gamma \int_0^{2\pi} d\phi \Phi_\gamma(E_\gamma, \theta, \phi), \quad (17)$$

where $\Phi_\gamma(E_\gamma, \theta, \phi)$ is obtained from eq. (10).

From fig. 6 one can see that a large anisotropy is predicted for the type I scenario. The curves plotted there refer to the case of $m_\chi = 100$ GeV and $\langle\sigma v\rangle = 3 \times 10^{-27} \text{cm}^3/\text{s}$. The solid, dashed and dotted lines refer to NFW, Moore and SIS profiles respectively, while the thick curve is the contribution to the gamma ray flux due to the smooth component in the direction defined by $\cos\theta$.

In fig. 7, we plot the same curves for the scenario of type II. The anisotropies obtained in this case are clearly smaller than the previous case, as indicated by the almost flat lines. This is due to our conservative assumption that there are no clumps in the inner 10 kpc of the Galaxy. In this case, the contribution of the clumps to the gamma-ray flux is never dominant over the smooth component for clumps with NFW profile, while for the SIS clumps emission is always dominant. For clumps with Moore profile, the clumpy component overcomes the smooth component in the region around the Galactic anticenter.

5. Conclusion

The annihilation of dark matter in the halo of our galaxy generates a diffuse background of gamma-rays. The dark matter substructure of the galactic halo can be a dominant component of the diffuse gamma-ray flux depending on the concentration and location of DM clumps in the inner regions of the Galactic halo.

In order to bracket the range of possible fluxes, we considered two extreme scenarios, that we named type I and type II. The first corresponds to extremely concentrated clumps present everywhere in the Galaxy halo, while in the second scenario the clumps are much less concentrated and are completely destroyed by tidal effects in the inner 10 kpc of the Galaxy. While the type I scenario allows one to put very strong constraints on the properties of neutralinos and on the density profile inside clumps, the type II scenario generates fluxes

of diffuse gamma-rays which are barely detectable, with the exception of the case in which the density profile of the clumps is modeled as a SIS sphere.

For the type I scenario, most of the parameter space of neutralino dark matter is ruled out if the density profile of dark matter clumps is in the form of a SIS sphere or a Moore profile. Weaker bounds can be imposed on the neutralino parameter space in the case of NFW density profile.

Recent N-body simulations have started to gather evidence of the destruction of clumps in the inner regions of dark matter halos, which favor type II like scenarios. On the other hand, numerical simulations only resolve relatively high mass clumps and the distribution of more concentrated smaller clumps is yet to be understood, although there is some recent progress in this direction (Berezinsky, Dokuchaev and Eroshenko 2003). Finally, one should keep in mind the possibility of detecting isolated nearby clumps with Atmospheric Cherenkov telescopes (Tasitsiomi and Olinto 2002), which may be more promising than looking at diffuse fluxes.

Acknowledgments

We thank A. Kravtsov, F. Stoehr, and R. Wechsler for many helpful discussions. This work was supported in part by the Center for Cosmological Physics at the University of Chicago through grant NSF PHY-0114422, by the NSF through grant AST-0071235 and DOE grant DE-FG0291-ER40606 at the University of Chicago, and by the Italian Minister of Research through Cofin 2002.

REFERENCES

- T. Baltz, L. Bergström, J. Edsjo, P. Gondolo and P. Ullio, Dark SUSY review (2002), www.physto.se/~edsjo/darksusy.
- V. Berezinsky, V. Dokuchaev and Y. Eroshenko, preprint astro-ph/0301551.
- V. Berezinsky, A.V. Gurevich, and K.P. Zybin, Phys.Lett. **B294** (1992) 221.
- V. Berezinsky, A. Bottino, and G. Mignola, Phys.Lett. **B325** (1994) 136.
- L. Bergström, J. Edsjö, P. Gondolo, and P. Ullio, Phys.Rev. **D59** (1999) 043506.
- L. Bergström, J. Edsjö and P. Ullio, Phys.Rev.Lett. **87** (2001) 251301.

- G. Bertone, G. Sigl, and J. Silk, MNRAS **326** (2001) 799.
- P. Blasi, and R.K. Sheth, Phys.Lett. **B486** (2000) 233.
- P. Blasi, A.V. Olinto, C. Tyler, Astropart. Phys. 18 (2003) 649-662.
- C. Calcáneo-Roldán and B. Moore, Phys.Rev. D62 (2000) 123005.
- A. Cesarini, F. Fucito, A. Lionetto, A. Morselli, and P. Ullio, *preprint* astro-ph/0305075
- J. Ellis, K.A. Olive, Y. Santoso, and V.C. Spanos, Phys.Lett. B565 (2003) 176-182
- S. Ghigna, B. Moore, F. Governato, G. Lake, T. Quinn and J. Stadel, MNRAS **300** (1998) 146.
- P. Gondolo and J. Silk, Phys.Rev.Lett. **83** (1999) 1719.
- P. Gondolo, Phys. Lett. B494 (2000) 181-186.
- P.Gondolo, J. Edsjo, L.Bergstrom, P.Ullio, E.A. Baltz, DarkSusy, <http://www.physto.se/~edsjo/darksusy> (2002).
- K. Hagiwara et al. (Particle Data Group), Phys.Rev. **D66** (2002) 010001.
- C.T. Hill, Nucl.Phys. **B224** (1983) 469.
- G. Jungman, M. Kamionkowski, and K. Griest, Phys.Rep. **267** (1996) 195.
- A. Klypin, A.V. Kravtsov, O. Valenzuela and F. Prada, Astrophys.J. **522** (1999) 82.
- D.A. Kniffen, D.L. Bertsch, and N. Gehrels, “GeV-TeV Gamma Ray Astrophysics Workshop”, Snowbird, UT. AIP Proc. Conf. **515** (1999) 492.
- D. Merritt and M. Milosavljevic, in DARK 2002: 4th International Heidelberg Conference on Dark Matter in Astro and Particle Physics, 4-9 Feb 2002, Cape Town, South Africa, H.V. Klapdor-Kleingrothaus, R. Viollier (eds.), *preprint* astro-ph/0205140.
- B. Moore, S. Ghigna, F. Governato, G. Lake, T. Quinn, J. Stadel and P. Tozzi, Astrophys.J. **524** (1999) L19.
- J.F. Navarro, C.S. Frenk and S.D.M. White, Astrophys.J. **462** (1996) 563; *ibid.* **490** (1997) 493.
- C. Power, J.F. Navarro, A. Jenkins, C.S. Frenk, S.D.M. White, V. Springel, J. Stadel, and T. Quinn, Mon. Not. Roy. Astron. Soc. 338 (2003) 14-34.

P. Salucci, MNRAS **320** (2001) L1-L5.

P. Sreekumar et al., Astrophys.J. **494** (1998) 523.

F. Stoehr, S.D.M. White, G. Tormen, and V. Springel, MNRAS, 335 (2002) L84.

A. Tasitsiomi and A. V. Olinto, Phys.Rev. **D66** (2002) 083006.

A. Tasitsiomi, *preprint* astro-ph/0205464.

C. Tyler, Phys.Rev. **D66** (2002) 023509.

L. Bergstrom, J. Edsjo, and P. Ullio, Phys. Rev. Lett. 87 (2001) 251301

P. Ullio, L. Bergström, J. Edsjö and C. Lacey, Phys.Rev. **D66** (2002) 123502.

R.H. Wechsler, J.S. Bullock, J.R. Primack, A.V. Kravtsov and A. Dekel, Proceedings of the Marseille 2001 Conference, Treyer and Tresse, eds.